NORSAR

NORSAR Scientific Report No. 1-2000/2001

Semiannual Technical Summary

1 April - 30 September 2000

Frode Ringdal (ed.)

Kjeller, November 2000

6.6 Source properties and focal depth of the M_S 4.2 Revda (Lovozero) earthquake of August 17, 1999

Introduction

Between mid May and end of September,1999, 13 Lennartz MARSlite data loggers equipped with three-component LE-3D/5s broad band seismometers with a sampling rate of 125 Hz were in operation over an area of about 200 km NS and 350 km EW in Finnmark (see Fig. 6.6.1). The purpose of the experiment, which was conducted in cooperation with the University of Potsdam, was partly to study possible earthquakes along the prominent postglacial Stuoragurra fault in Masi (Olesen 1988; Bungum and Lindholm, 1996; Dehls et al., 2000), and partly to study regional seismicity and associated source and attenuation characteristics, including events from mines on the Kola peninsula.

More details about this experiment can be found in Schweitzer (1999).

Fig. 6.6.1 shows the Masi-1999 stations together with the background seismicity from this region (based on Bungum and Lindholm, 1996), including available focal mechanisms. The red circle with a focal mechanism is a local earthquake at the Stuoragurra fault on August 22, 1999, recorded during this experiment, while the Revda earthquake of August 17, 1999 can be seen with a focal mechanism in the southeastern corner of the map. Both of these events are analyzed in this report, the former for anelastic attenuation (Q) and the latter for source properties and focal depth.

The Revda earthquake - observed data from the Masi-1999 network

This Revda (Lovozero) earthquake at M_L 3.9 and M_S 4.2-4.3 (Schweitzer, 1999) was the strongest of the local and regional earthquakes observed during the Masi-1999 field experiment. Fig. 6.6.2 shows the Masi recordings of this event, together with an indication of the regional phases observed, including Pn, Sn, Lg and Rg. The data plotted are corrected for frequency response and bandpass filtered between 0.01 and 50 Hz. The distance range is from 286 to 553 km as seen in the figure.

To present the character and the potentials of the broadband data more clearly we have in Fig. 6.6.3 included the original (vertical) record for channel MA06 (distance 472 km) on top, while further below we have filtered the recording sequentially with one octave wide bandwidth filters between 0.05 and 50 Hz. The contribution of the different wave groups to the seismic signal becomes obvious from this display, in that:

- for frequencies up to 1 Hz the surface wave Rg is dominant,
- between 1 and 8 Hz the signal is mainly composed by the Lg and Sn wave group, and
- for frequencies above 8 Hz the signal is dominated by scattering.

The low-frequency Rg wave is sensitive to the velocity-depth distribution of the upper part of the crust. The arrival time for Rg increases with frequency indicating both a pronounced dispersion and a corresponding strong velocity gradient within the crust. With increasing fre-

quency the seismic waves become sensitive to 2D and 3D small-scale heterogeneities within the crust resulting in multiple scattering.

Fig. 6.6.4 shows the displacement spectra of the Revda earthquake for 12 of the Masi stations, corrected for the instrument response. The signal amplitude spectra are drawn as solid lines, and the corresponding noise spectra as computed for a 120 s time window preceding the signal onset are indicated by dotted lines. For all stations, the signals are above the noise for frequencies higher than 0.1 Hz, going at least up to 10 Hz.

The displacement spectra in Fig. 6.6.4 are relatively flat up to about 0.7 Hz and then decay with a slope of about -3 with frequency. For frequencies larger than 1 Hz the stations MA02, MA03, MA09, MA10 and MA12 exhibit frequency peaks which have been identified unambiguously as station effects, tied to the fact that all of these stations are installed on soil sites. Typically these stations are located on top of thin (up to 10 m) sedimentary layers consisting of moraines, which are known to have strong tuning effects for frequencies at about 10Hz (NORSAR and NGI, 1998). The spectra for stations located on solid rock, MA04, MA06, MA07, MA08 and MA13, are all characterized by a relatively simple shape.

Q estimation based on the Masi M_L 2.7 earthquake of August 22, 1999

The purpose of the Masi-1999 experiment with respect to the earthquakes that we hoped to get from the Stuoragurra faults was fulfilled in that several, albeit small, events were recorded over the four months of operation (about what one statistically should expect). The largest of these was a M_L 2.7 earthquake on August 22, 1999, used in the following for estimation of anelastic attenuation (Q).

The response corrected spectra for the Masi event all show similar characteristics as just described for the Revda event, in particular with respect to soil versus rock sites. The rock station spectra are relatively flat up to 10 Hz, which is to be expected since the corner frequency should be expected to be at least at that level for a M_L 2.7 earthquake.

In consequence of this the spectra of the rock stations were analyzed for an average Q in the frequency range between 1 and 10 Hz. The analysis is based on an iterative method, which adjusts Q and station corrections simultaneously in order to match the average level of the amplitude spectra, making the procedure independent of assumptions on geometrical spreading. The result is a relatively high Q of about 1400. Furthermore, it turned out that the station correction for the rock stations are almost negligible.

Fig. 6.6.5 displays the Q-corrected spectra of the rock stations. The spectra now have almost the same level between 1 and 10 Hz, reducing significantly the Q-related roll-off at high frequencies.

The derived Q corrections are also applied to the spectra of the non-rock (moraine) sites. The difference of these spectra from the average level of the rock sites provides frequency-dependent station corrections which will be used in the subsequent analysis of the August 17, 1999, Revda (Lovozero) earthquake in order to compensate for the tuning (soil response) effects.

Full waveform modelling of the Revda earthquake

Full waveform modelling of this event has been conducted using two different methods, a precise frequency-wavenumber (f-k) method as coded by Ray Haddon, and the reflectivity method (Müller, 1985). Both methods compute complete seismograms for 1D velocity models. One difference between the two methods is the implementation of the source. The f-k method computes synthetic seismograms for specified distributions of slip over spatially extensive source regions. In the implementation of the program that we have been using, the particular specified slip distributions are kinematic representations that very closely represent the classical exact elastodynamic dislocation solutions for a circularly symmetric crack in a homogeneous elastic medium for constant stress drop (see, e.g., Madariaga, 1976). For numerical integration purposes, the perfectly continuous slip distribution was discretized. For the modelling with the reflectivity method we used a moment tensor point source with a source function describing a smooth increase of the seismic moment (Brüstle and Müller, 1983).

The main target of the modelling has been the dispersed surface waves and the goal was to resolve the 1D crustal shear wave velocity model and the source depth of the Revda event. In the following we present a few selected modelling results pointing out the effect of different source depths (Fig. 6.6.6) and crustal structure (Table 6.6.1).

Fig. 6.6.6 shows firstly the focal mechanism solution used as a starting point for the synthetics. To this end we used first motion readings from altogether 28 stations, including the MASI-1999 stations and stations from Kola, Finland, Sweden and Norway (denoted as circles and filled squares), resulting in a number of possible solutions. The shaded fault plane solution is the final double-couple solution obtained through a systematic search over mechanism parameter space during the waveform modelling. As a part of this, the seismic moment, the source radius and stress drop were obtained by detailed matching of the source spectrum, which in turn was estimated by averaging all observed spectra after applying the station- and Q-corrections inferred from the analyses of the August 22, 1999, earthquake mentioned above.

We considered various velocity models in order to fit the observed waveforms; Table 6.6.1 shows two of them. Model 1 is a simple two layered crustal model with the Conrad discontinuity at 15 km depth and the Moho discontinuity at 40 km. Model 2, which represents our final model, has the same major discontinuities, but contains additionally a velocity gradient within the uppermost three kilometers. The P-wave velocities and densities are considered to be proportional to the S-wave velocity by a factor $\sqrt{3}$ and 0.7, respectively.

Fig. 6.6.7 shows the comparison of the observed data and the synthetics computed with the f-k method for the crustal model containing the velocity gradient (model 2) for stations MA04, MA06, MA07 and MA09. The results for the other stations are similar and therefore we omit displaying the corresponding plots. In order to match the spectra at the low-frequency end we assumed a circular fault plane with 1.6 km radius and a complete stress drop of 45 bars. The source depth in this case was 5 km. It is seen from the figure that the amplitude spectra of the observed data (solid lines), could be fitted quite well by the synthetics (dashed lines). The absolute values as well as the spectral shape of the individual components (green: vertical, blue: radial, red: transversal) could be modelled successfully within the frequency range from 0.1 to at least 1 Hz. The misfit for frequencies above about 1.5 Hz is a result of chosen discretization.

A better fit at least up to 6 Hz can be achieved by a refinement of the discretization. However, the refinement is associated with additional computational efforts, and the main purpose of this study was to model the low-frequency surface waves.

The bottom part of Fig. 6.6.7 displays the fit of the waveforms. The seismograms are bandpass-filtered between 0.1 and 0.5 Hz and the components are shifted vertically for a better comparision. The synthetics (black) and the observed data (color coded) are scaled in the same way and the lineup is according to the absolute time. The arrival times, the amplitudes and the dispersion of the radial (blue) and vertical (green) component (containing the Rg contribution) are well matched by the synthetics. The fit of the transverse (red) component (containing mainly the Lg-wave group) is sufficient for station MA04, but for the more distant stations (MA06, MA07 MA09) there is a phase shift of about 1.5 s. Such a misfit was consistently present in our modelling results. It was not possible to match the arrival times of Rg and Lg simultaneously using a 1D-velocity model.

Figs. 6.6.8 to 6.6.11 illustrate the effects of different velocity models and of variations in source depth. The synthetics in these cases were computed using the reflectivity method. Fig. 6.6.8 represents the results for the simple two-layered crustal model. The spectra could be modelled reasonably well for frequencies up to 1 Hz. The differences for higher frequencies are seen to be somewhat larger in this case as compared to the f-k method, which is mainly due to the somewhat simpler source function used in the reflectivity modelling. The duration of the source function was chosen as 1 s which results in the lack of high frequency energy. This, however, does not affect our waveform modelling, where we primarily are interested in matching the surface waves in the observed seismograms at low frequencies.

The bottom part of Fig. 6.6.8 again shows the fit of the observed (colored) and synthetic (black) waveform components. Generally the fit is unsatisfactory, because the synthetics exhibit no dispersion. This is of course due to the simple crustal velocity model, which in this case consists of only two homogeneous layers. In order to model the dispersion of the observed data it is necessary to include a velocity variation with depth. We performed various numerical experiments to this end and concluded with a model containing a fairly strong velocity gradient (model 2, Table 6.6.1) as the one which gave the best fit to the observations.

Figs. 6.6.9 and 6.6.10 show the results for crustal model 2 and a focal depth of 2.5 and 7.5 km, respectively. The main effect of a change of the source depth is on the spectra. At the first order, a decrease of the source depth by a factor two results in a frequency doubling of the spectral peak of Rg. This is clearly illustrated in Fig. 6.6.9, where the amplitude spectra of the synthetics are shifted to higher frequencies and the fit between modelled and observed data becomes worse. For a focal depth at 7.5 km (Fig. 6.6.10) the spectra are shifted to lower frequencies, and the observed spectra are slightly underestimated.

The effect of the focal depth on the waveforms is mainly expressed in the duration of the surface wave groups. For the shallow source the synthetics exhibit a multi-cyclic behavior with a gradual decay within a time window of about 15 s. In the case of a source depth of 7.5 km, the synthetics appear to be less dispersive.

Fig. 6.6.11 shows the results for our preferred model 2 with a source depth of 5 km. This results are comparable to those displayed in Fig. 6.6.7, because the same velocity model was used in the two cases. Differences are due to the source models.

The waveform fit of the Rg wave (radial and vertical component) is almost perfect in Fig. 6.6.11, reproducing both the arrival times, the amplitudes and the dispersion characteristics of the observations. The discrepancies for the transverse component remain to be explained. Timing differences between the transverse and radial/vertical components is, however, a common and well known problem for structural modelling using Lg and Rg waves. Anisotropy is often suggested as a possible cause for this phenomenon, but a velocity shift related to small-scale lateral heterogeneities (Müller et al., 1992; Roth et al., 1993) may also contribute to such effects.

From the waveform modelling of the surface waves of the Revda earthquake we conclude that the source depth of the event was deeper than 2.5 km, probably between 4 and 7 km, and that there must be a relatively strong velocity gradient in the uppermost crust.

M. Roth
H. Bungum
R.A.W. Haddon

References

Brüstle, W. and G. Müller (1983): Moment and duration of shallow earthquakes from Love-wave modelling for regional distances. *Phys. Earth Planet. Inter.*, 32, 312-324.

Bungum, H. and C. Lindholm (1997): Seismo- and neotectonics in Finnmark, Kola, and the southern Barents Sea, Part 2: Seismological analysis and seismotectonics. *Tectonophysics*, 270, 15-28.

Dehls, J.F., O. Olesen, L. Olsen and L.H. Blikra (2000): Neotectonic faulting in northern Norway; the Stuoragurra and Normannvikdalen postglacial faults. *Quat. Sci. Rev.*, 19, 1447-1460.

Madariaga, R. (1976): Dynamics of an expanding circular fault. *Bull. Seism. Soc. Am.*, 66, 639-666.

Müller, G. (1985): The reflectivity method: a tutorial. *J. Geophys.*, 58, 153-174.

Müller, G., M. Roth and M. Korn (1992): Seismic-wave traveltimes in random media. *Geophys. J. Int.*, 110, 29-41.

Olesen, O. (1988): The Stuoragurra fault, evidence of neotectonics in the Precambrian of Finnmark, northern Norway. *Nor. Geol. Tidsskr.*, 68, 107-118.

Roth, M., G. Müller and R. Snieder (1993): Velocity shift in random media. *Geophys. J. Int*, 115, 552-563.

Schweitzer, J. (1999). The MASI-1999 field experiment. *In* F. Ringdal (ed.): *Semiannual Technical Report 1 April - 30 September 1999*. NORSAR Sci. Report 1-1999/2000, Kjeller, Norway, pp. 91-101.

Schweitzer, J., F. Krüger, G. Richter, E. Hicks, C. Lindholm and H. Bungum (2000). The 1999 Finnmark seismic field experiment. *In* J. Dehls and O. Olesen (eds.): *Neotectonics in Norway, Annual Technical Report 1999*. NGU (Norwegian Geological Survey) Report 2000.001, pp. 89-97.

Table 6.6.1: Crustal models used in the waveform modeling. Model 1 represents a simple two-layered crust, whereas model 2 includes a strong velocity gradient approximated by thin constant velocity layers. The P-wave velocities and densities are related to the S-wave velocity (β) via the factor 3 and 0.7, respectively.

Crustal Model 1		Crustal Model 2	
Depth (km)	β (km/s)	Depth (km)	β (km/s)
0 - 15	3.65	0 - 0.75	3.25
15 - 40	3.80	0.75 - 1.5	3.35
> 40	4.65	1.5 -2.25	3.45
		2.25 - 3	3.55
		3 - 15	3.65
		15 - 40	3.80
		> 40	4.65

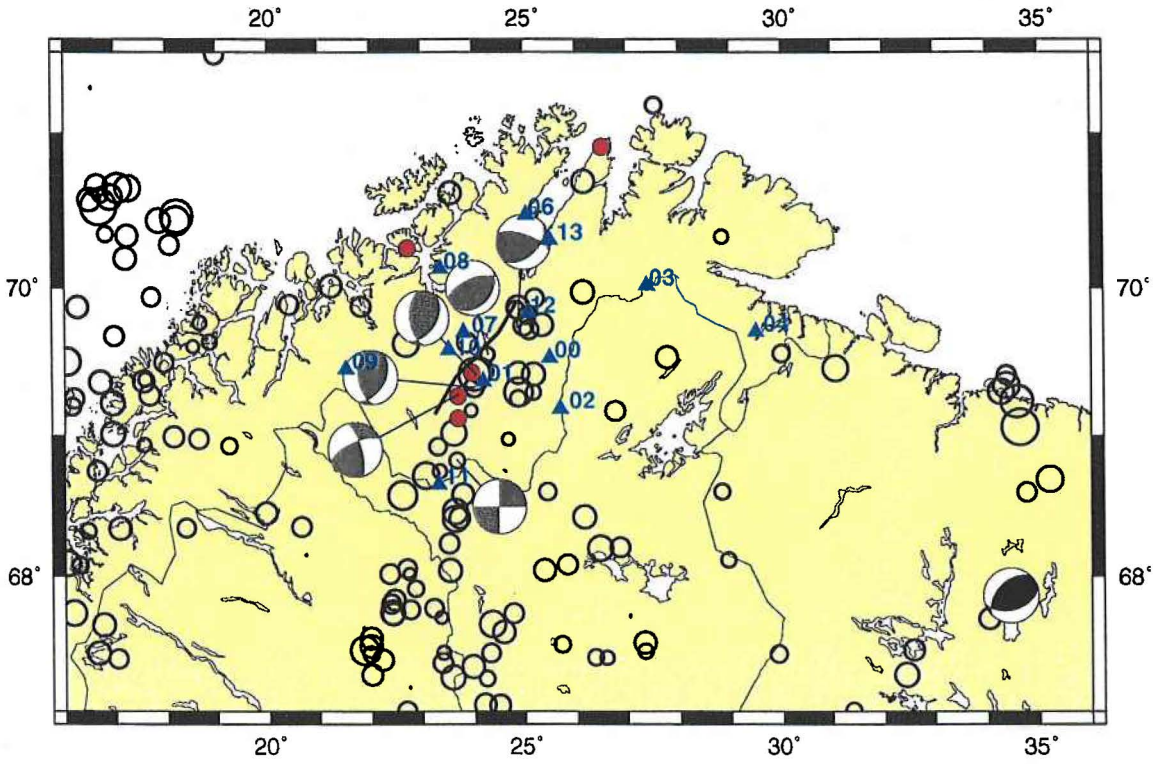

Fig. 6.6.1. The Masi-1999 stations (blue triangles with numbers) together with previous earthquakes in Finnmark for the time period 1979-1992 (Bungum and Lindholm, 1996), updated with earthquakes for the time period 1993-1999 (all with open circles) and preliminary locations from the Masi-1999 network (red circles). Available focal mechanism solutions are also shown, including the M_L 2.7 Masi earthquake of August 22, 1999 (69.276N. 23.685E), used in this study for estimation of Q, and the August 17, 1999, Revda earthquake (67.865N, 34.454E) at the Kola peninsula, which is the focus of the present study. Redrawn from Schweitzer et al. (2000).

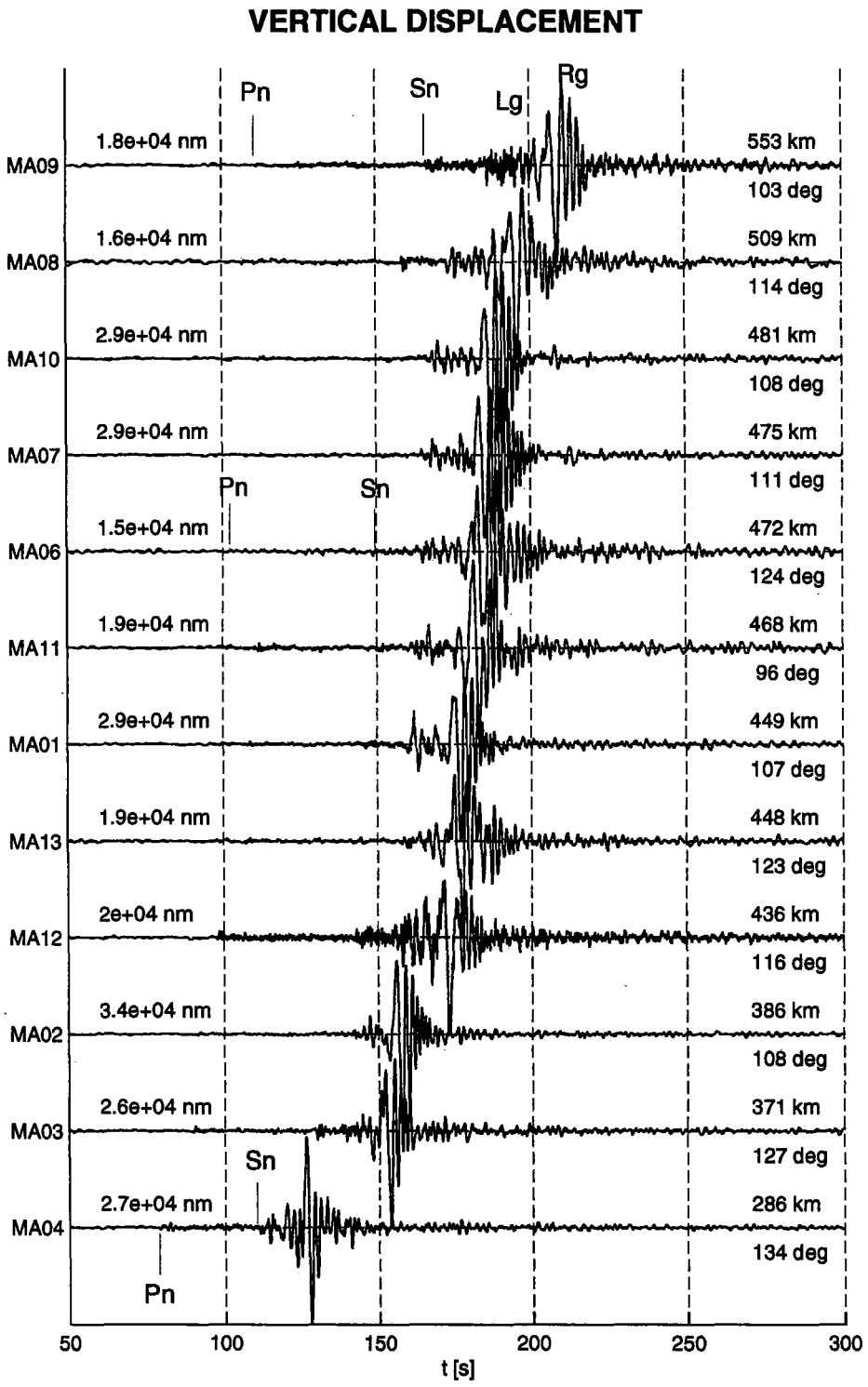

Fig. 6.6.2. Vertical displacement recorded at the stations of the MASI-1999 network for the Revda earthquake. The seismograms are corrected for the instrument response and bandpass filtered between 0.01Hz and 50Hz. The time axis starts at 4:44:50. On the right hand side the epicentral distances and back azimuths are annotated, on the left hand side the trace maximum in units of nm.

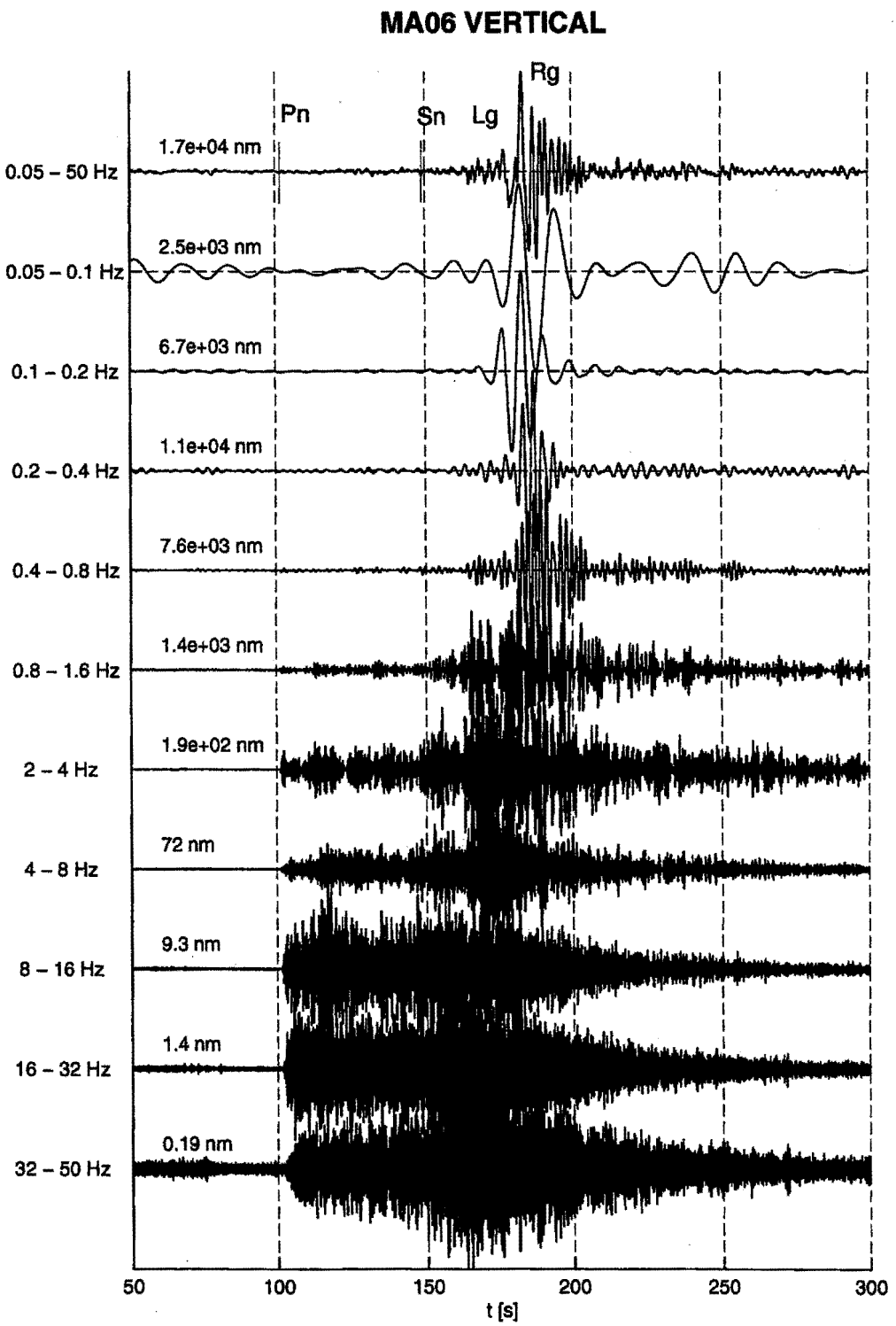

Fig. 6.6.3. Displacements recorded at station MA06 for different frequency bands. See the main text for more details and discussion.

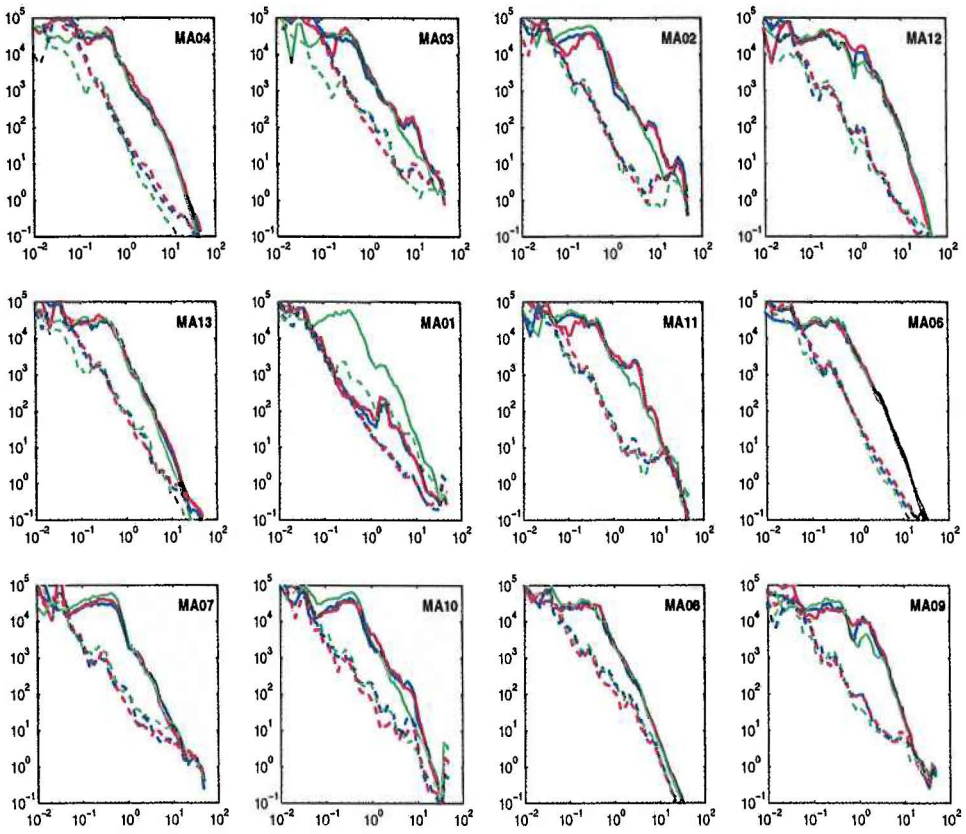

Fig. 6.6.4. Signal (solid lines) and noise (dashed lines) amplitude spectra of the Revda event. The spectra of the three components (vertical: green, radial: blue, transverse: red) are plotted in units of [nm s] versus frequency in [Hz]. The spectra indicate a good signal-to-noise ratio between 0.1 and 10 Hz. The corner frequency of the event is at about 0.7 Hz.

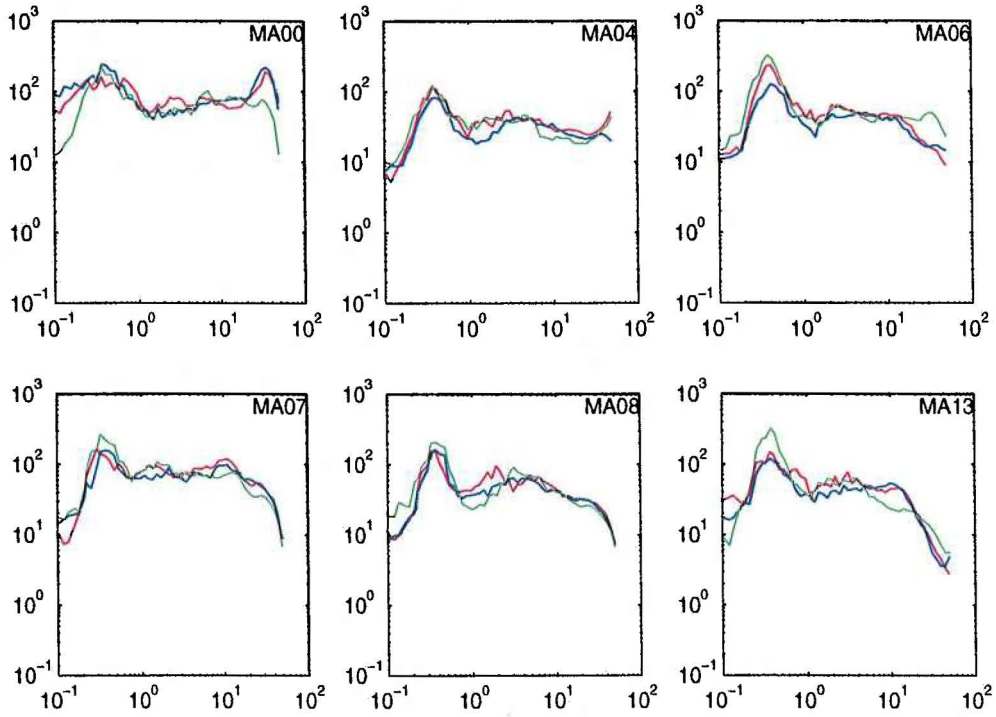

Fig. 6.6.5. Q-corrected spectra for the August 22, 1999, Masi earthquake at the rock sites. The spectra of the three components (red: transverse, blue: radial, green: vertical) are plotted in units of [nm s] versus frequency in [Hz].

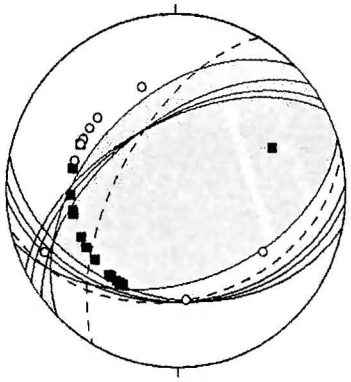

$M_0 = 6x10^{22}$ dyn-cm ($M_W = 4.5$)

Strike = 240°, dip = 60°, rake = 70°

Focal depth = 2.5, 5, 7.5 km

Source radius = 1.6 km (rupture area 8 km^2)

Stress drop $\Delta\sigma$ = 45 bars

Fig. 6.6.6. This figure shows the initial focal mechanism solution for the Revda event derived from 28 first motion readings from Fennoscandia (filled symbols are compressions, open symbols dilatations), with several possible solutions (courtesy of Erik Hicks), used as starting solution for the waveform modelling. The shaded solution is the final one following a systematic search over mechanism parameter space. The parameters for the final solution are shown to right.

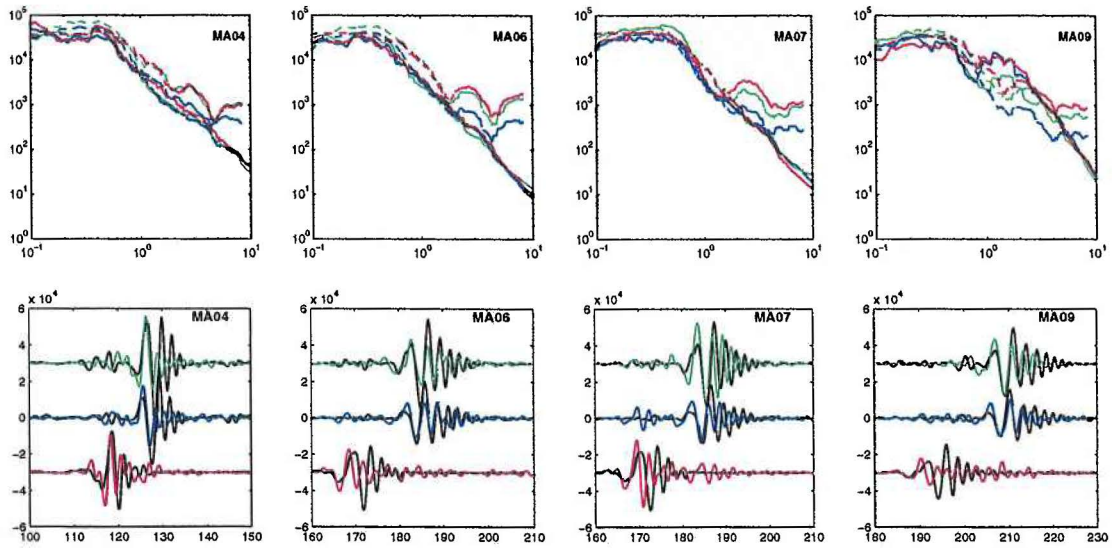

Fig. 6.6.7. Observations and synthetics for model 2 and a source depth of 5 km computed with the f-k method. Top: signal (solid) and modelled (dashed) amplitude spectra (in [nm s]) for the frequency range between 0.1 and 10 Hz, Green, blue and read are the vertical, radial and transverse component, respectively. Bottom: Observed displacement (color coded as above) and modelled displacement (black)

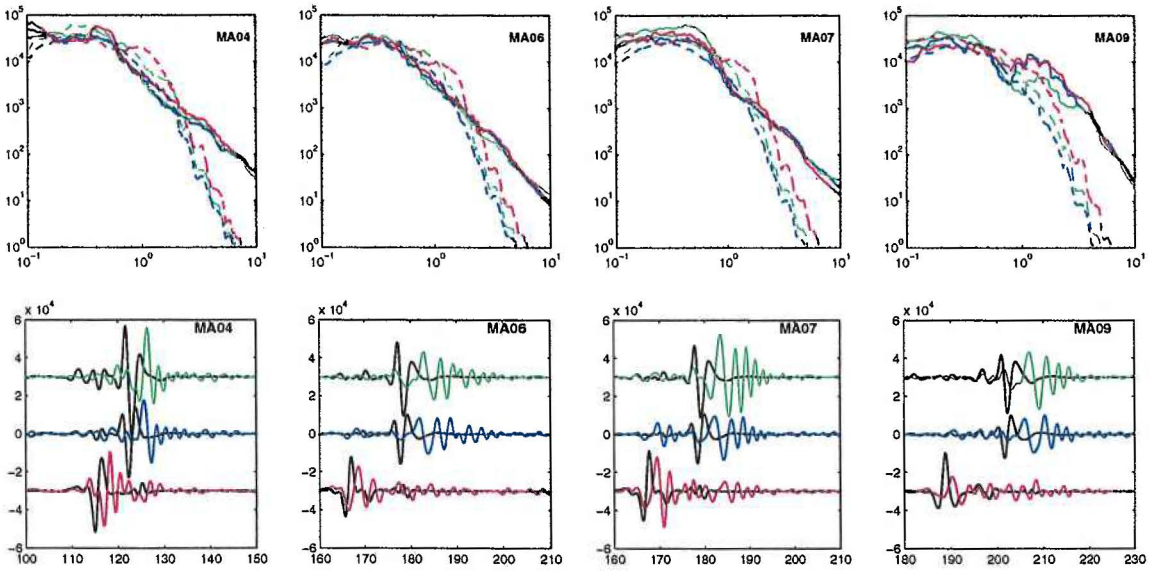

Fig. 6.6.8. Observations and synthetics for model 1 with 5km source depth computed with the reflectivity method (color coding as in Fig. 6.6.7).

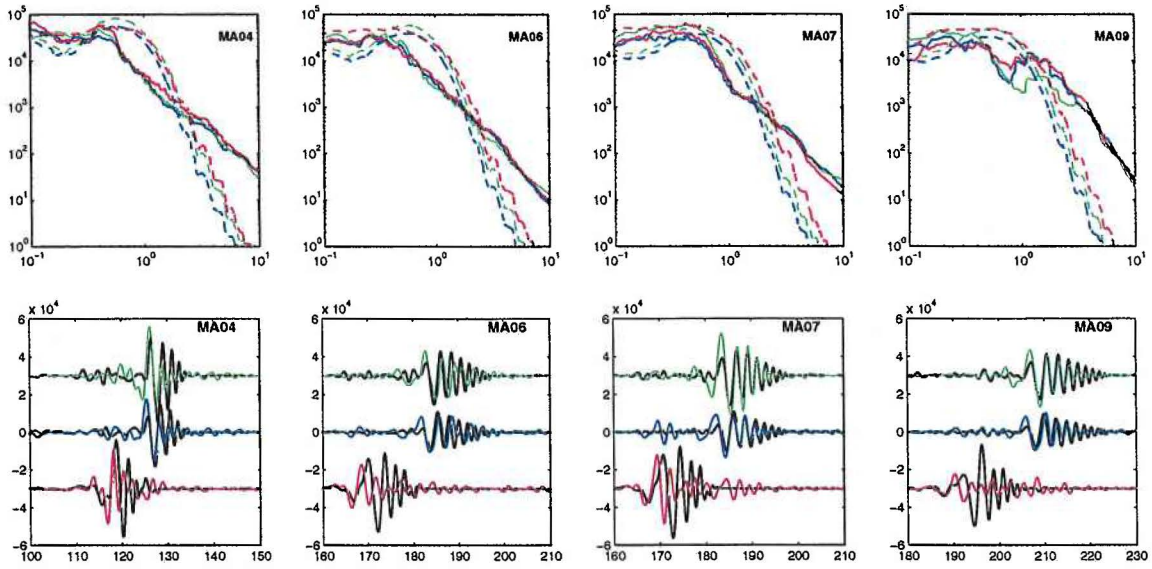

Fig. 6.6.9. Observations and synthetic for crust model 2 and a source depth of 2.5 km computed with the reflectivity method (color coding as in Fig. 6.6.7).

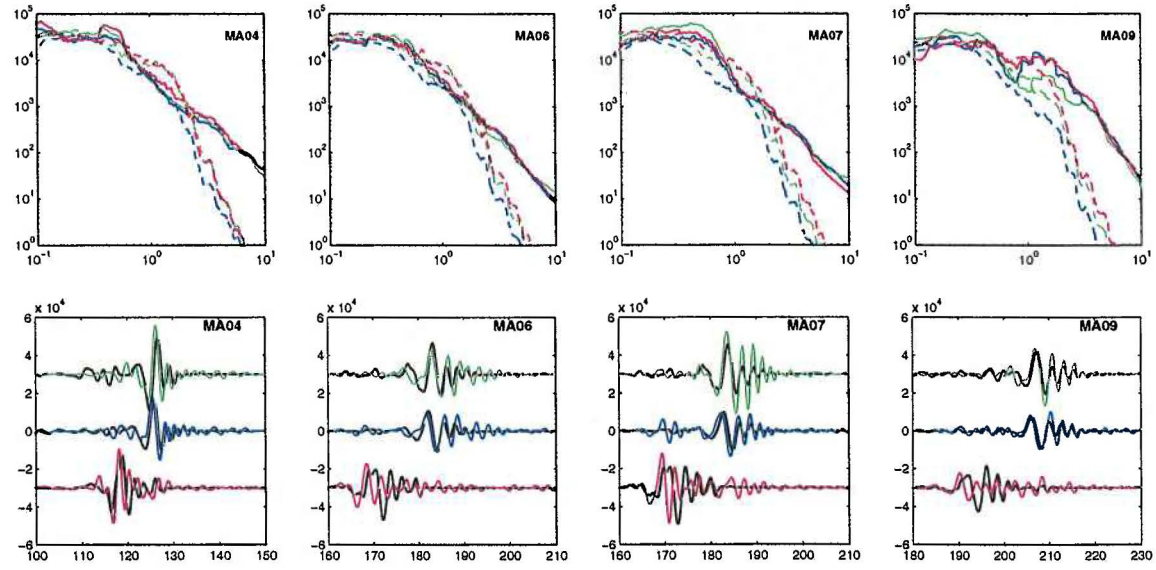

Fig. 6.6.10. Observations and modelling for crust model 2 and a source depth of 7.5 km computed with the reflectivity method (color coding as in Fig. 6.6.7).

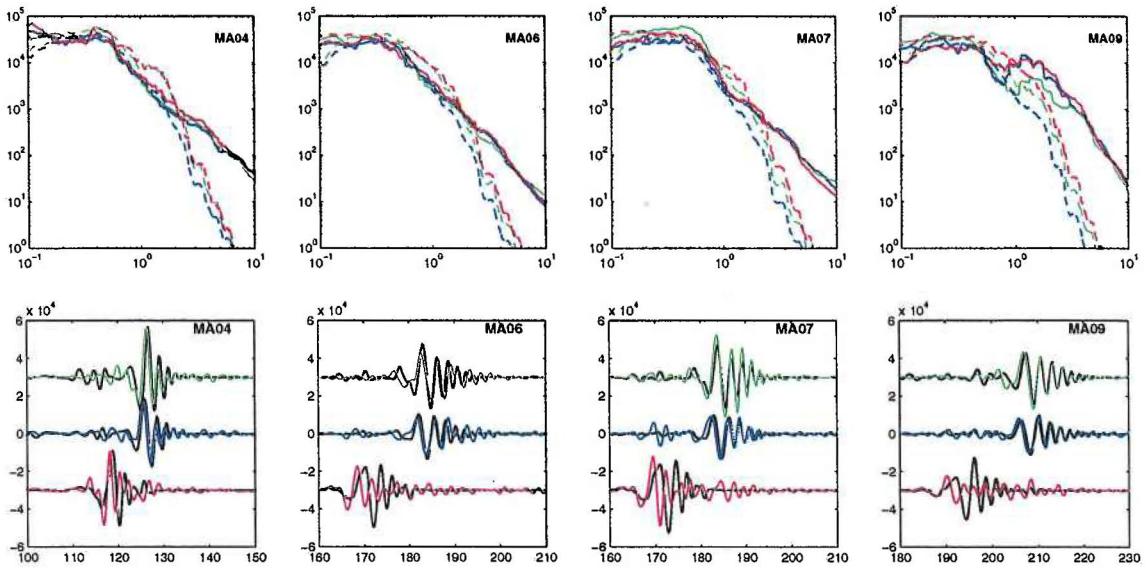

Fig. 6.6.11. Observations and synthetics for model 2 and 5km source depth computed with the reflectivity method (color coding as in Fig. 6.6.7).